Intelligent GNSS Positioning using 3D Mapping and Context Detection for Better Accuracy in Dense Urban Environments

Paul D Groves, Mounir Adjrad, Han Gao and Claire Ellul
University College London

BIOGRAPHY

Dr Paul Groves is a Senior Lecturer (associate professor) at UCL, where he leads a program of research into robust positioning and navigation within the Space Geodesy and Navigation Laboratory (SGNL). He joined in 2009, after 12 years of navigation systems research at DERA and QinetiQ. He is interested in all aspects of navigation and positioning, including improving GNSS performance under challenging reception conditions, advanced multisensor integrated navigation, and novel positioning techniques. He is an author of more than 80 technical publications, including the book *Principles of GNSS, Inertial and Multi-Sensor Integrated Navigation Systems*, now in its second edition. He holds a bachelor's degree and doctorate in physics. (p.groves@ucl.ac.uk)

Dr Mounir Adjrad is a Postdoctoral Research Associate at University College London (UCL). His current research interests are on Intelligent Urban Positioning (IUP) exploiting conventional GNSS technology augmented by 3D models of urban environments. He has multidisciplinary research experience in industry and academic institutions working on topics such as ultra-wideband technology, GNSS, satellite engineering, radar, biomedical engineering and transport engineering He holds a State Engineering degree in electronics, Magister in signal and communication, and State Doctorate in signal and systems from Ecole Nationale Polytechnique d'Alger, Algeria. (mounir.adjrad@ucl.ac.uk)

Han Gao is a PhD student at University College London (UCL) in the Engineering Faculty's Space Geodesy and Navigation Laboratory (SGNL). He received a Bachelor's degree in Aerospace Engineering from Shanghai Jiao Tong University (SJTU) in 2014. He is interested in multi-sensor contextual navigation and positioning techniques. (han.gao.14@ucl.ac.uk)

Dr Claire Ellul is a Reader (associate professor) at UCL, specializing in Three-Dimensional Geographical Information Science (3D GIS), with a particular interest in 3D usability – including rendering and analytical (topological) performance of large 3D city models on mobile devices and real-world applications of 3D GIS. Prior to becoming an academic, she spent 10 years as a GIS consultant and systems integration specialist.

ABSTRACT

Conventional GNSS positioning in dense urban areas can exhibit errors of tens of meters due to blockage and reflection of signals by the surrounding buildings. Here, we present a full implementation of the intelligent urban positioning (IUP) 3D-mapping-aided (3DMA) GNSS concept. This combines conventional ranging-based GNSS positioning enhanced by 3D mapping with the GNSS shadow-matching technique. Shadow matching determines position by comparing the measured signal availability with that predicted over a grid of candidate positions using 3D mapping. Thus, IUP uses both pseudo-range and signal-to-noise measurements to determine position. All algorithms incorporate terrain-height aiding and use measurements from a single epoch in time.

Two different 3DMA ranging algorithms are presented, one based on least-squares estimation and the other based on computing the likelihoods of a grid of candidate position hypotheses. The likelihood-based ranging algorithm uses the same candidate position hypotheses as shadow matching and makes different assumptions about which signals are direct line-of-sight (LOS) and non-line-of-sight (NLOS) at each candidate position. Two different methods for integrating likelihood-based 3DMA ranging with shadow matching are also compared. In the position-domain approach, separate ranging and shadow-matching position solutions are computed, then averaged using direction-dependent weighting. In the hypothesis-domain approach, the candidate position scores from the ranging and shadow matching algorithms are combined prior to extracting a joint position solution.

Test data was recorded using a u-blox EVK M8T consumer-grade GNSS receiver and a HTC Nexus 9 tablet at 28 locations across two districts of London. The City of London is a traditional dense urban environment, while Canary Wharf is a modern environment. The Nexus 9 tablet data was recorded using the Android Nougat GNSS

receiver interface and is representative of future smartphones. Best results were obtained using the likelihood-based 3DMA ranging algorithm and hypothesis-based integration with shadow matching. With the u-blox receiver, the single-epoch RMS horizontal (i.e., 2D) error across all sites was 4.0 m, compared to 28.2 m for conventional positioning, a factor of 7.1 improvement. Using the Nexus tablet, the intelligent urban positioning RMS error was 7.0 m, compared to 32.7 m for conventional GNSS positioning, a factor of 4.7 improvement.

An analysis of processing and data requirements shows that intelligent urban positioning is practical to implement in real-time on a mobile device or a server.

Navigation and positioning is inherently dependent on the context, which comprises both the operating environment and the behaviour of the host vehicle or user. No single technique is capable of providing reliable and accurate positioning in all contexts. In order to operate reliably across different contexts, a multi-sensor navigation system is required to detect its operating context and reconfigure the techniques accordingly. Specifically, 3DMA GNSS should be selected when the user is in a dense urban environment, not indoors or in an open environment. Algorithms for detecting indoor and outdoor context using GNSS measurements and a hidden Markov model are described and demonstrated.

1. INTRODUCTION

This work was first presented at ION GNSS+ 2016 [1][2]. Further details of 3DMA GNSS and context determination are presented in [1] and [2], respectively

The positioning performance of global navigation satellite systems (GNSS) in dense urban areas is poor because buildings block, reflect and diffract the signals. If the real-time position accuracy using low-cost equipment could be improved to 5m or better, a host of potential applications would benefit. These include situation awareness of emergency, security and military personnel and vehicles; emergency caller location; mobile mapping; tracking vulnerable people and valuable assets; intelligent mobility; location-based services; location-based charging; augmented reality; and enforcement of curfews, restraining orders and other court orders. A further accuracy improvement to around 2m would also enable navigation for the visually impaired; lane-level road positioning for intelligent transportation systems; aerial surveillance for law enforcement, emergency management, building management and newsgathering; and advanced rail signaling.

Buildings and other obstacles degrade GNSS positioning in three ways. Firstly, where signals are completely blocked, they are simply unavailable for positioning, degrading the signal geometry. Secondly, where the direct signal is blocked (or severely attenuated), but the signal is received via a (much stronger) reflected path, this is known as non-line-of-sight (NLOS) reception. NLOS signals exhibit positive ranging errors corresponding to the path delay (the difference between the reflected and direct paths). These are typically a few tens of meters in dense urban areas, but can be much larger if a signal is reflected by a distant building. Thirdly, where both direct line-of-sight (LOS) and reflected signals are received, multipath interference occurs. This can lead to both positive and negative ranging errors, the magnitude of which depends on the signal and receiver designs. NLOS reception and multipath interference are often grouped together and referred to simply as "multipath". However, to do so is highly misleading as the two phenomena have different characteristics and can require different mitigation techniques [3].

There are many different approaches to multipath and NLOS mitigation [4]. A good GNSS antenna is more sensitive to right-hand circularly polarized (RHCP) signals than to left-hand circularly polarized (LHCP) signals. As direct LOS signals are RHCP while most reflected signals are LHCP or mixed polarization, this reduces multipath errors by attenuating the reflected signal components with respect to the direct. Furthermore, NLOS reception can usually be detected from the signal to noise ratio (SNR) measurements, enabling NLOS signals to be eliminated from the position calculation. However, cheaper antennas offer less polarization discrimination and smartphone antennas none at all.

Much of the literature on multipath mitigation is dominated by receiver-based signal-processing techniques [5]. However, because they work by separating out the direct and reflected signals within the receiver, they can only be used to mitigate multipath; they have no effect on NLOS reception at all. Consistency checking selects the most consistent subset of the signals received to compute a position solution from. This is based on the principle that measurements from "clean" direct LOS signals produce a more consistent navigation solution than those from NLOS and severely multipath-contaminated signals. In dense urban areas, a subset comparison approach is more robust that conventional sequential testing [6].

Over the past six years, there has been a lot of interest in 3D-mapping-aided (3DMA) GNSS, a range of different techniques that use 3D mapping data to improve GNSS positioning accuracy in dense urban areas. The simplest form of 3DMA GNSS is terrain height aiding. For most land applications, the antenna is at a known height above the terrain. By using a digital terrain model (DTM), also known as a digital elevation model (DEM), the position solution may be constrained to a surface. In conventional least-squares positioning, this is done by generating a virtual ranging measurement [7]. By effectively removing a dimension from the position solution, this improves the accuracy of the remaining dimensions. In open areas, terrain height aiding only improves the vertical position solution (as one might expect). However, in dense urban

areas where the signal geometry is poor, it can improve the horizontal accuracy by almost a factor of two [8].

3D models of the buildings can be used to predict which signals are blocked and which are directly visible at any location [9][10]. This can be computationally intensive. However, the real-time computational load can be reduced dramatically by using building boundaries [11]. These describe the minimum elevation above which satellite signals can be received at a series of azimuths and are precomputed for each candidate position. A signal can then be classified as LOS or NLOS simply by comparing the satellite elevation with that of the building boundary at the corresponding azimuth.

The shadow-matching technique [12] determines position by comparing the measured signal availability and strength with predictions made using a 3D city model over a range of candidate positions. Several research groups have demonstrated this experimentally, using both single and multiple epochs of GNSS data [13][14][15][16][17] [18][19][20]. Cross-street position accuracies of a few meters have been achieved in dense urban areas, enabling users to determine which side of the street they're on. This complements GNSS ranging, which is more accurate in the along-street direction in these environments because more direct LOS signals are received along the street than across it. Shadow matching has also been demonstrated in real time on an Android smartphone [21]. A review of shadow matching, including its error sources and how it could be developed further may be found in [22].

3D models of the buildings can also be used to aid conventional ranging-based GNSS positioning. Where the user position is already approximately known, it is straightforward to use a 3D city model to predict the NLOS signals and eliminate them from the position solution [23][24][25]. However, for most urban positioning applications there is significant position uncertainty. One solution is to define a search area centered on the conventional GNSS position solution and compute the proportion of candidate positions at which each signal is receivable via direct LOS. This can then be used to re-weight a least-squares position solution and aid consistency checking [8]. More sophisticated approaches which score position hypotheses using the GNSS pseudo-range measurements and satellite visibility predictions at each candidate position are presented in [26] and in Section 2.2 of this paper.

Several groups have extended 3D-mapping-aided GNSS ranging by using the 3D city model to predict the path delay of the NLOS signals across an array of candidate positions [27][28][29][30]. A single-epoch positioning accuracy of 4m has been reported [29]. However, unless the search area is small, this approach is very computationally intensive as the path delay cannot easily be pre-computed. The urban trench approach presented in [31] enables the path delays of NLOS signals to be computed very efficiently, but only if the building layout is highly symmetric, so it can only be used in suitable environments. Therefore, NLOS path delay predictions are not used in the work presented here.

3DMA GNSS ranging has also been combined with 'direct positioning' which uses the receiver correlator outputs to score an array of position hypothesis [32].

Clearly, to get the best performance out of GNSS aided by 3D mapping, as much information as possible should be used. Thus, both pseudo-range and SNR measurements from a multi-constellation GNSS receiver should be used, together with both LOS/NLOS predictions and terrain height from 3D mapping. This concept is known as intelligent urban positioning (IUP) [33].

A preliminary implementation of the IUP concept is presented in [34]. This integrates shadow matching with a 3DMA least-squares GNSS ranging algorithm incorporating terrain height aiding, consistency checking, and weighting of the pseudo-ranges according to the average predicted satellite visibility over a search area. Position-domain integration is used with two different weighting approaches. Error covariance-based weighting was found to perform slightly better than weighting using the street azimuth. The overall root mean square (RMS) horizontal (i.e., 2D) single-epoch position accuracy obtained using a u-blox EVK M8T receiver was 6.1 m, compared to 25.9 m using conventional GNSS positioning, a factor of four improvement.

This paper extends this work, incorporating:

- A 3DMA GNSS ranging algorithm based on computing the likelihood of an array of candidate position hypotheses based on the satellite visibility predictions at each position (the least-squares algorithm is retained for initialization);
- Hypothesis-domain integration of 3DMA ranging with shadow matching;
- Additional test sites in the Canary Wharf area of London, which is similar to modern urban environments in North America and Asia;
- Test results using a Nexus 9 tablet equipped with the Android Nougat GNSS receiver interface that will enable 3DMA GNSS ranging to be implemented on a smartphone.

All results presented here are based on a single epoch of GNSS measurements, which suits many location-based service (LBS) applications that require a quick one-time fix. 3DMA GNSS is particularly important for single-epoch positioning because other augmentations, such as carrier-smoothing, carrier-phase positioning and integration with inertial sensors, only work with multiple epochs of GNSS data [4].

An alternative implementation of the intelligent urban positioning concept is presented in [26]. The shadow-matching algorithm is simpler than that used here. A different likelihood-based 3DMA GNSS ranging algorithm is also implemented which uses only the signals predicted

to be direct LOS at each candidate position. The experimental tests demonstrate that the method works well. However, as the results presented combine measurements from multiple epochs, they are not directly comparable with the single-epoch results presented here.

Extending the IUP implementation presented here to multiple epochs for navigation and tracking applications is a subject for future work. Better performance can be expected as several researchers have already demonstrated that filtering can improve 3DMA GNSS performance [19][20][26]. Conventional GNSS positioning also works much better with multiple epochs of data. With an extended Kalman filter (within which carrier-smoothing is normally inherent), it is much easier to detect outliers due to NLOS reception and severe multipath interference than it is using single-epoch least-squares positioning. However, 3DMA GNSS also has an important role to play in multi-epoch positioning as it will enable carrier-smoothed, inertially aided and potentially even real-time kinematic (RTK) carrier-phase positioning to be accurately initialized and re-initialized in challenging urban environments.

The IUP algorithms are designed for outdoor positioning in dense urban areas. They do not work indoors and are not needed in open areas where conventional GNSS positioning works well. To determine when to use IUP, it is thus necessary to detect the environmental context. Indoor-outdoor context detection has been demonstrated using both GNSS [35][36][37][38] and Wi-Fi [37][38][39]. However, GNSS-based approaches were found to be more reliable. Therefore, here GNSS-based indoor-outdoor context detection is developed further here. A full implementation of context-adaptive navigation should also consider behavioural context and its association with environmental context [2] [37][38].

Section 2 summarizes the 3DMA GNSS positioning algorithms, including the least-squares and likelihood-based 3DMA ranging algorithms, the shadow matching algorithm and the integration algorithms. Section 3 presents experimental test results from data collected using a u-blox EVK M8T consumer-grade GNSS receiver and a Nexus 9 tablet at 28 locations across two districts of London. Section 4 then discusses the practicality of real-time implementation of intelligent urban positioning. Section 5 describes environmental context detection using GNSS signals. Finally, Sections 6 and 7 summarize the conclusions and plans for future work, respectively.

2. 3DMA GNSS POSITIONING ALGORITHMS

The intelligent urban positioning system comprises four main algorithms as shown in Figure 1. The least-squares 3DMA GNSS ranging algorithm is used to initialize the likelihood-based 3DMA GNSS ranging algorithm and the shadow-matching algorithm, enabling them to use a much smaller search area than if the conventional GNSS position was used for initialization. The integration algorithms then compute a joint position solution from likelihood-based 3DMA ranging and shadow matching. Both a position-domain integration algorithm and a hypothesis-domain integration algorithm are presented. The least-squares 3DMA GNSS ranging solution is also integrated with shadow matching in the position domain to enable comparison of the new IUP algorithms with those presented in [34]. Thus, three integrated position solutions are produced altogether. The following subsections summarize each algorithm.

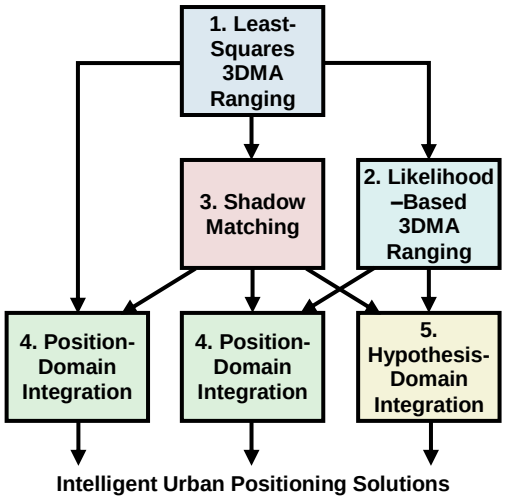

Figure 1: Intelligent urban positioning algorithm configuration

2.1. Least-Squares 3DMA GNSS Ranging

The least-squares 3DMA ranging algorithm comprises the following six steps:

1. A search area is determined using the conventional GNSS position solution on the first iteration and the previous solution on subsequent iterations, together with an appropriate confidence interval.
2. Using 3D mapping converted to precomputed building boundaries, the proportion of the search area within which each satellite is directly visible is computed, giving the probability that the signal is direct LOS.
3. A consistency-checking process is applied to the ranging measurements, using the direct LOS probabilities from the 3D mapping.
4. The set of signals resulting from the consistency checking process is subjected to a weighting strategy based on the previously determined LOS probabilities and carrier-power-to-noise-density ratio, C/N_0.
5. Terrain height is extracted from the 3D mapping and a virtual range measurement is generated using the position at the centre of the search area.
6. Finally, a position solution is derived from the pseudo-ranges and virtual range measurement using weighted least-squares estimation.

The algorithm is then iterated several times to improve the position solution. Full details are presented in [8] (final version) and [40] (preliminary version).

2.2. Likelihood-based 3DMA GNSS Ranging

In likelihood-based 3DMA GNSS ranging an array of candidate position hypotheses are scored according to the correspondence between the predicted and measured pseudo-ranges. This enables different error distributions to be assumed for a given GNSS signal at different candidate positions. Thus, at positions where a signal is predicted from the 3D mapping (via precomputed building boundaries), to be NLOS, a skew normal (Gaussian) distribution is assumed, biased towards positive ranging errors. Elsewhere, a conventional symmetric normal distribution is assumed.

Terrain height aiding is inherent in generating the position hypotheses, enabling a single height to be associated with each horizontal position and thus avoiding the computational load of a 3D search area. The receiver clock bias is eliminated by differencing all pseudo-range measurements across satellites.

Other likelihood-based 3DMA GNSS ranging algorithms based on candidate position hypothesis scoring have been described in the literature. However, they differ from the approach proposed here. In [28] and [29], pseudo-ranges predicted to be NLOS are corrected using path delays predicted from the 3D mapping. This is potentially more accurate, but the path delay computation is highly computationally intensive. In [26], a least-squares position solution is computed using only those signals predicted to be direct LOS and the candidate position is then scored according to its Mahalanobis distance from the least-squares position solution.

The likelihood-based 3D-model-aided ranging algorithm comprises the following six steps:

1. A circular search area of radius 40m is defined with its centre at the least-squares 3DMA ranging position solution. Within this search area, a grid of candidate positions is set up with a spacing of 1m.
2. For each candidate position, the satellite visibility is predicted using the building boundaries precomputed from the 3D city model. At each candidate position, the highest elevation satellite predicted to be direct LOS is selected as the reference satellite.
3. At each candidate position, the direct LOS range to each satellite is computed. Measurement innovations are then computed by subtracting the computed ranges from the measured pseudo-ranges and then differencing with respect to the reference satellite.
4. At each candidate position, the measurement innovation for each satellite predicted to be NLOS is re-mapped to a skew normal distribution.
5. A likelihood score for each candidate position is computed using the vector of measurement innovations and the measurement error covariance matrix.
6. A position solution is derived by using the likelihood scores to weight the candidate positions.

Further details are presented in [1], while full details of the algorithm will be presented in a forthcoming journal submission, currently under preparation.

2.3. Shadow Matching

The shadow matching algorithm is a modified version of that presented in [18]; further details are presented in [1]. The shadow matching algorithm comprises the following five steps:

1. A circular search area of radius 40m is defined with its centre at the least-squares 3DMA ranging position solution. Within this search area, a grid of candidate positions is set up is set up with a spacing of 1m.
2. For each candidate position, the satellite visibility is predicted using the building boundaries precomputed from the 3D city model. If the satellite elevation is above the building boundary at the relevant azimuth, the LOS probability predicted from the building boundary, $p(LOS|BB)$, is set to 0.85. Otherwise, it is set to 0.2. These values allow for diffraction and 3D model errors.
3. The observed satellite visibility is determined from the GNSS receiver's C/N_0 or signal to noise ratio (SNR) measurements. From these, a probability that each received signal is direct LOS is estimated.
4. Each candidate position is scored according to the match between the predicted and measured satellite visibility. The overall likelihood score for each position is then the product of the individual satellite probabilities.
5. A position solution is derived by using the likelihood scores to weight the candidate positions.

2.4. Position-Domain Integration

The position-domain integration algorithm uses the error covariance matrices of the 3DMA ranging and shadow matching position solutions to compute a weighted average of the two positions.

For least-squares 3DMA GNSS ranging, the error covariance is calculated using the weighting matrix and measurement matrix then transformed from Cartesian ECEF to Easting and Northing components.

For shadow matching and likelihood-based 3DMA ranging, an initial error covariance is computed from the second statistical moments of the likelihood surface. The likelihood surface is non-Gaussian and potentially multimodal. The error covariance is therefore adjusted to account for multimodal distributions by rescaling it according to the kurtoses along the maximum- and minimum-covariance directions.

Further details are presented in [1] and full details in [34].

2.5. Hypothesis-Domain Integration

Both shadow matching and likelihood-based 3DMA ranging can produce multimodal position distributions where there is a good match between predictions and measurements in more than one part of the search area.

These will typically comprise the true position hypothesis and one or more false hypotheses. In general, the true position hypothesis will be consistent across the two positioning methods whereas the false hypotheses will not be. Hypothesis-domain integration therefore helps to eliminate false position hypotheses by computing a joint ranging and shadow matching likelihood surface by multiplying the ranging and shadow-matching likelihoods for each candidate position, then computing a position solution by using the joint likelihood scores to weight the candidate positions. Further details are presented in [1].

3. 3DMA GNSS EXPERIMENTAL RESULTS

GNSS measurements, comprising GPS and GLONASS, were collected in August 2016 using a u-blox EVK M8T GNSS receiver and a HTC Nexus 9 tablet. U-blox data collection was performed by interfacing the receiver to a Raspberry Pi (via USB) for data logging, where this latter was powered by a battery pack and configured as a WiFi hotspot to which a smartphone was connected (using the mobile SSH App) to configure the system and enable data logging. Figure 2 illustrates the u-blox-based hardware.

The Nexus 9 data collection was performed using a purposely written App capturing both NMEA sentences as well as GNSS "raw data", including GNSS satellite pseudo-ranges. This latter was possible as the tablet was running the latest Android operating system, version 7.0, also known as Nougat. The tablet device is illustrated in Figure 3. The tablet's GNSS receiver and antenna are similar to those found on smartphones, so the results should be a good prediction of the performance of smartphones compatible with the Nougat GNSS interface.

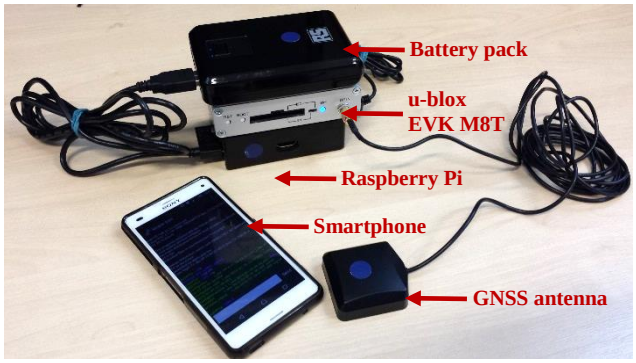

Figure 2. U-blox EVK M8T-based data logging hardware.

Figure 3. Nexus 9 tablet running Android 7.0 (Nougat) Operating System and a dedicated App for raw GNSS data logging.

Two rounds of data collection were performed using both devices at two different sites: at 18 locations in the City of London and 10 locations in Canary Wharf. Figures 4–7 illustrate these sites. The City of London area is typical of a traditional European city with narrow streets and buildings packed close together. The Canary Wharf area is representative of a modern city environment, found more commonly in North American and East Asian cities. The streets are wider and the buildings taller with more space between them. There is also a greater ratio of glass and steel to brick and stone than in the City of London district.

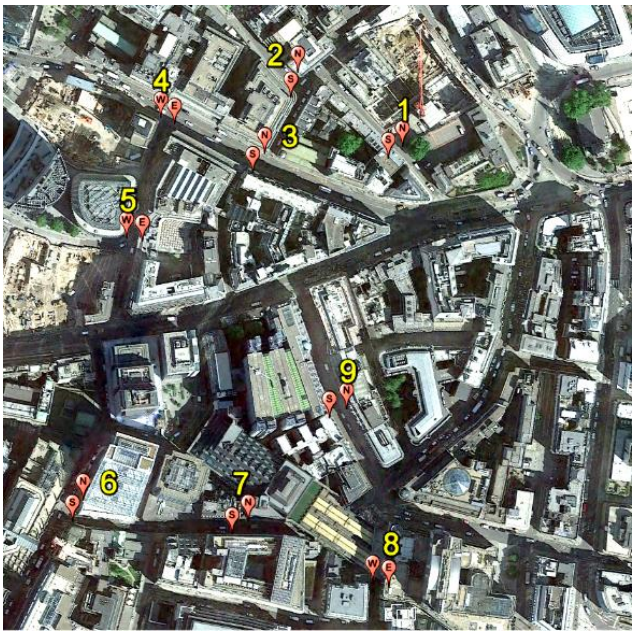

Figure 4. Data collection sites in the City of London (GoogleTM earth).

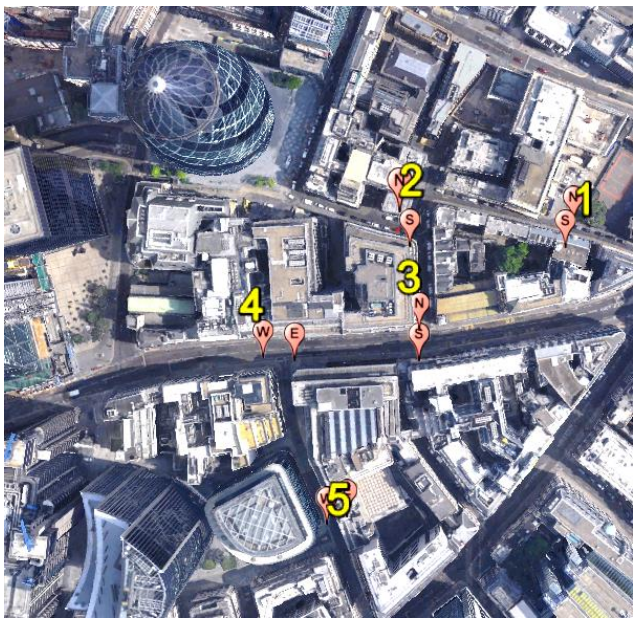

Figure 5. Part of data collection sites in the City of London – 3D view (GoogleTM earth).

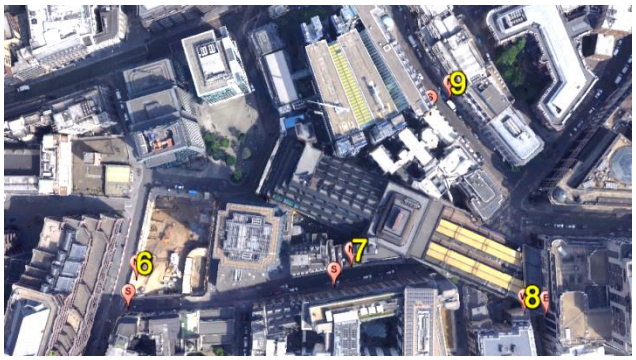

Figure 6. Part of data collection sites in the City of London – 3D view (GoogleTM earth).

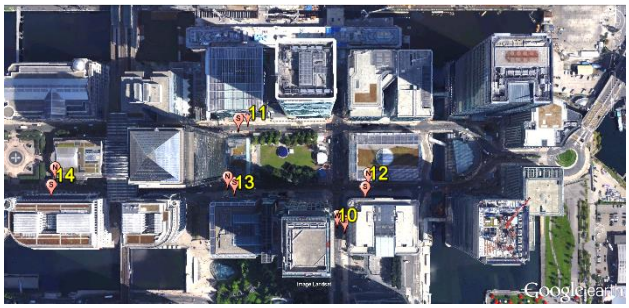

Figure 7. Data collection sites in the Canary Wharf area - London – 3D view (GoogleTM earth).

All tablet data collection was collocated with the corresponding u-blox data collection. The sites were paired with data collected on opposite sides of the street on the edge of the footpath next to the road. The truth was established to decimeter-level accuracy using a 3D city model to identify landmarks and tape measure to measure the relative position of the user from those identified landmarks. The two rounds of data at each site were separated by approximately 2 hours, ensuring that the satellite positions in the two datasets were independent. The first dataset was used for calibrating the shadow-matching algorithm. The second dataset was then used for testing the positioning algorithms. 4 minutes of data were collected at each site on each round.

A 3D city model of the area, from Ordnance Survey (OS), was used to generate the building boundary data used for the subsequent analysis. The model is stored in the Virtual Reality Modelling Language (VRML) format. Figures 8 and 9 illustrate the 3D model used in this study.

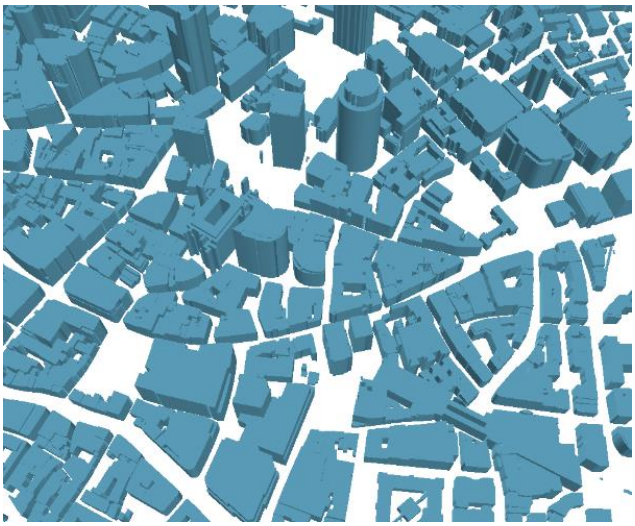

Figure 8. The 3D model of City of London used in the experiments.

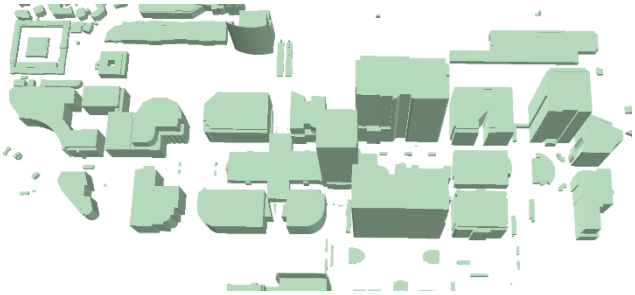

Figure 9. The 3D model of Canary Wharf used in the experiments.

Figures 10 and 11 shows the combined RMS errors across all sites for each positioning method using the u-blox EVK M8T and HTC Nexus 9 tablet running Android 7.0 (Nougat), respectively. Results for individual sites are presented in [1].

It can be clearly seen that likelihood-based 3DMA ranging outperforms least-squares 3DMA ranging. Comparing 3DMA ranging with shadow matching, it can be seen that both ranging algorithms are more accurate in the along-street direction, while shadow matching is more accurate in the across-street direction. This is effect is greater at the City of London sites than at the Canary Wharf sites. This because there is a much greater different between along-

street and across-street geometry in the City of London than at Canary Wharf.

The integrated solution is much more accurate than 3DMA ranging or shadow matching alone with hypothesis-domain integration 5-10% more accurate than position-domain integration.

The Nexus 9 results are not as good as the u-blox results, with conventional GNSS positioning affected least and shadow matching affected most. This is due to the inferior characteristics of a tablet (or smartphone) antenna, compared to the u-blox antenna. As the tablet antenna has no polarization discrimination, the direct LOS ranging measurements are subject to greater multipath interference and it is more difficult to distinguish LOS from NLOS signals using SNR measurements. Conventional positioning is least affected because it is dominated by the NLOS ranging errors that 3DMA positioning helps to minimize; these are not affected by the antenna design.

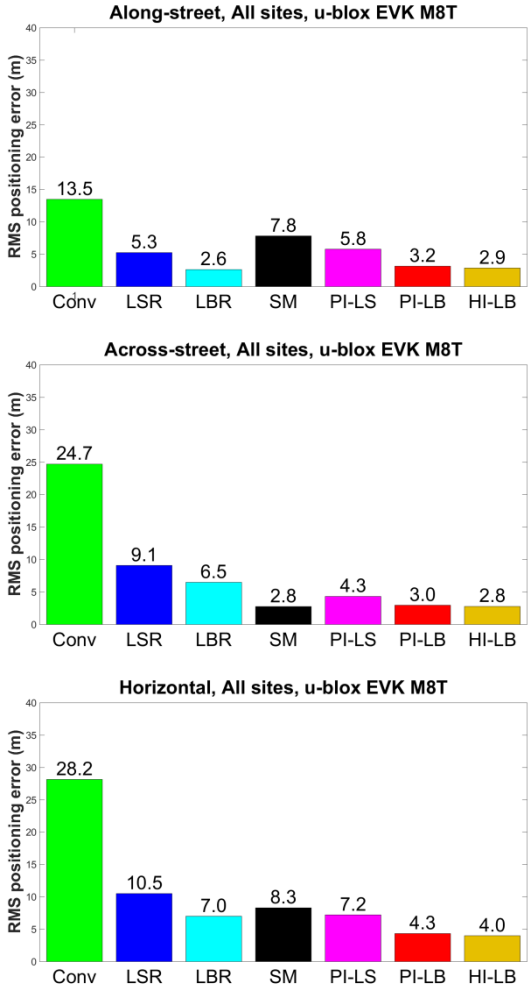

Figure 10. u-blox all sites across-street and overall horizontal RMS positioning error.

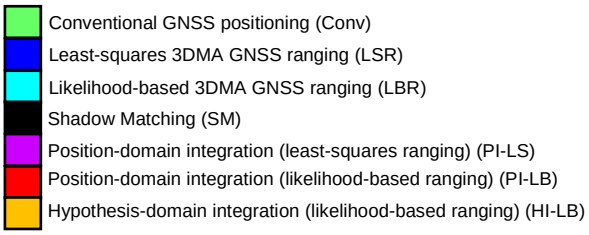

Legend for Figures 10 and 11.

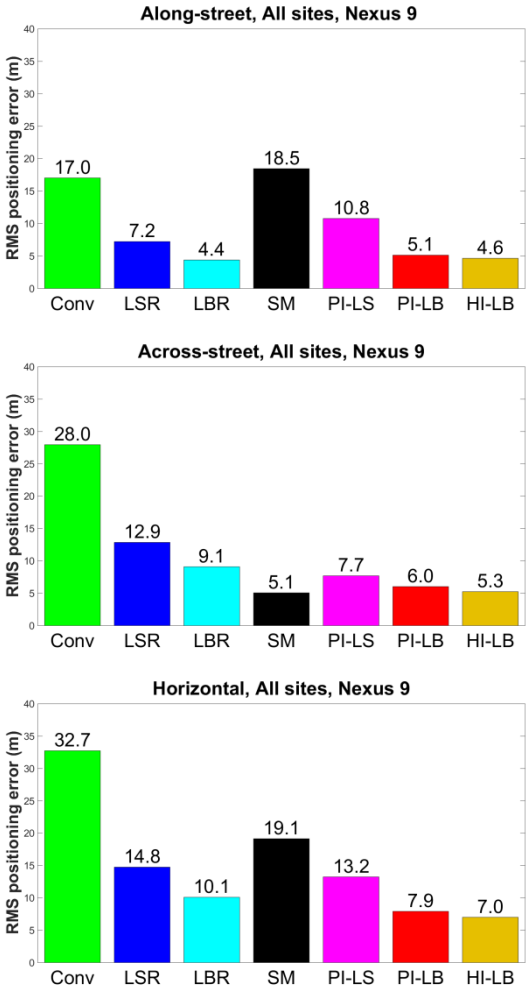

Figure 11. Nexus 9 all sites along-street, across-street and overall horizontal RMS positioning error.

Comparing the best solution, hypothesis-domain integration, with conventional GNSS positioning, it can be seen that intelligent urban positioning is a factor of 7.1 more accurate using the u-blox receiver and antenna and a factor of 4.7 more accurate using the Nexus 9 tablet.

4. PRACTICAL IMPLEMENTATION OF 3DMA GNSS

There are four ways in which 3D-mapping-aided GNSS, including the intelligent urban positioning algorithms presented here, could be implemented in a practical system:

- Post-processing of recorded data is suited to data collection applications such as mapping, and

monitoring the movement of people, animals or vehicles for research purposes.

- Real-time implementation on a remote server is suited to location-based services requiring a one-time position fix and to tracking applications with long update intervals.
- Real-time implementation on a mobile device using pre-loaded mapping data is suited to professional navigation and continuous tracking applications within a limited area.
- Real-time implementation on a mobile device using streamed mapping data is suited to consumer and professional navigation and continuous tracking applications.

A practical real-time implementation of any 3DMA GNSS system requires the following [41]:

- Real-time access to GNSS pseudo-range and SNR or C/N_0 measurements;
- Computationally efficient positioning algorithms;
- Access to 3D mapping data;
- A means of distributing the GNSS measurements and mapping data to the positioning algorithms.

Survey receivers have always provided the necessary GNSS measurements, but are not practical for most 3DMA GNSS applications. Obtaining them from consumer receivers has historically been problematic. However, today, receivers such as the u-blox M8T provide pseudo-range and SNR measurements from all GNSS constellations and a new interface provides access to this data through the application programming interface (API) on smartphones and tablets running the Android Nougat operating system that have a compatible GNSS chipset.

By using building boundaries instead of accessing the 3D mapping directly, the intelligent urban positioning algorithms presented here are able to run quickly. On a DELL Precision M2800 laptop computer (running the Microsoft Windows 7 operating system equipped with 16GB RAM and a quad-core processor with a 2.5GHz base frequency) it takes about 233 ms to compute a position solution from one epoch of GNSS measurement data. A new smartphone or tablet has 25–75% as much processing power as this laptop. Therefore, these algorithms should easily be able to run at 1 Hz on a mobile device.

CityGML (the Open Geospatial Consortium's approved standard for storage and exchange of virtual 3D city models, [42]) defines 3D city models as having varying levels of detail (LOD) [43]. LOD 0 is a digital terrain model, sometimes called a 2.5D model. LOD1 is a block model without any roof structures, i.e. all the buildings have flat roofs. Finally, LOD 2 is a full 3D city model having explicit roof structures and potentially associated texture.

City models are commonly stored using a boundary-representation approach, where each face (wall, floor, roof) of a building is described separately and a collection of faces grouped to represent the building. To minimize storage, these can be represented as polygons, described by the coordinates of each node (corner point). However, due to rounding errors this may not result in planar faces, which can cause problems for some of the techniques used to predict GNSS signal propagation, such as ray tracing. Thus, polygons are frequently triangulated, either on the fly or as a pre-processing stage, and a triangular mesh created prior to visualization or further processing. The greater the level of detail, the greater the number of triangles and hence the greater the time required for triangulation and the computational complexity of subsequent steps. Figures 12 and 13 show two 3D models of the same area of London, with Figure 12 derived from LOD 1 data and Figure 13 derived from LOD 2 data.

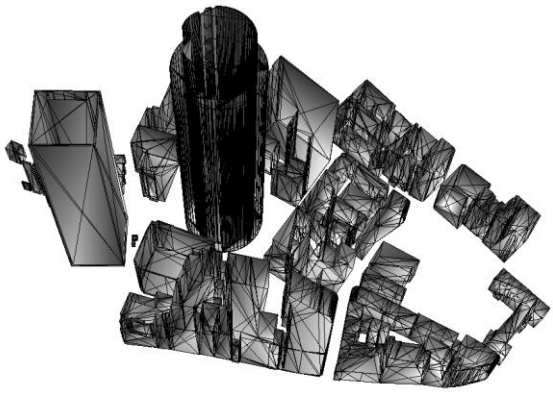

Figure 12. LOD 1 3D model of Central London near Fenchurch Street (data from Ordnance Survey)

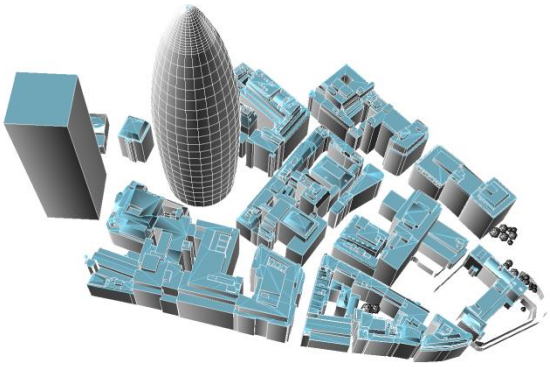

Figure 13. LOD 2 3D model of Central London near Fenchurch Street (data from Z Mapping)

Highly detailed 3D mapping is expensive. However, LOD 1 models are sufficient for most 3D-mapping-aided GNSS implementations. Open Street Map provides freely available building mapping for the world's major cities and many other places, much of it in 3D. Data is also available from national mapping agencies. Although coverage is not universal, it tends to be available in the dense urban areas where it is most needed.

This leaves data distribution. For server-based positioning, existing assisted GNSS interfaces can be used to transmit pseudo-range and SNR measurements from mobile devices to a server.

To run the positioning algorithms on a mobile device, mapping data is required. The terrain height data are easiest to handle. A 5m grid spacing is sufficient, corresponding to 40,000 points per km^2. 12 bits is sufficient to describe the relative height of a point within a tile, while 4 bytes are needed for the height of each tile's origin with respect to the datum. Thus, about 60 kB per km^2 is needed, so 1GB of storage could accommodate about 17,000 km^2 of data, much more with compression. Thus, this data could be pre-loaded in a mobile device.

Building boundaries require a lot more data. To a 1° precision, about 300 bytes are needed per building boundary. Assuming about half the space in a city is outdoor (building boundaries are not required for indoor locations), a 100×100m tile would require 1.5MB of data without compression, so 1GB of storage would only accommodate about 7 km^2 of data, maybe 70 km^2 with compression. Thus, pre-loading is only practical for users that operate within a relatively small area.

To stream building boundary data, only the search area is needed, which should be no bigger than 100×100m, considering only outdoor locations. Furthermore, only azimuths corresponding to the current set of GNSS satellites are needed, which reduces the amount of data required to 90kB without compression. Less than a kilobyte of terrain height data would be needed. 3G mobile download speeds are higher than 500 kB/s (4 Mbit/s). Therefore, streaming is easily practical and substantial data buffering could be accommodated to bridge gaps in communications coverage. Note that for continuous positioning, successive search areas will considerably overlap so it is not necessary to transmit a full set of mapping data at every epoch.

5. ENVIRONMENTAL CONTEXT DETECTION

To develop a GNSS-based environmental context determination algorithm, GNSS measurements were collected at 1 Hz from both GPS and GLONASS signals received by the smartphone. The data was collected at different locations of various indoor and outdoor environments, such as deep indoor, urban, outer indoor and open sky. About 200s of static data was collected at each site. Figure 14 presents histograms showing the normalised distributions of signal-to-noise ratio (SNR) measurements from four types of environment.

A number of trends may be identified from the histograms. A signal with a higher SNR is more likely to be LOS (Line-of-Sight) than NLOS (Non-Line-of-Sight). As expected, the average received SNR is lower in indoor environments than in deep urban and open sky environments, which is useful for environmental context detection. By comparing the GNSS SNR distributions, it can also be seen that the proportions of signals weaker than 25 dB-Hz vary between different environment types. Almost all the signals received in deep indoor environments are weaker than 25 dB-Hz while increasing proportions of signals stronger than 25 dB-Hz are observed for outer indoor, deep urban and open sky.

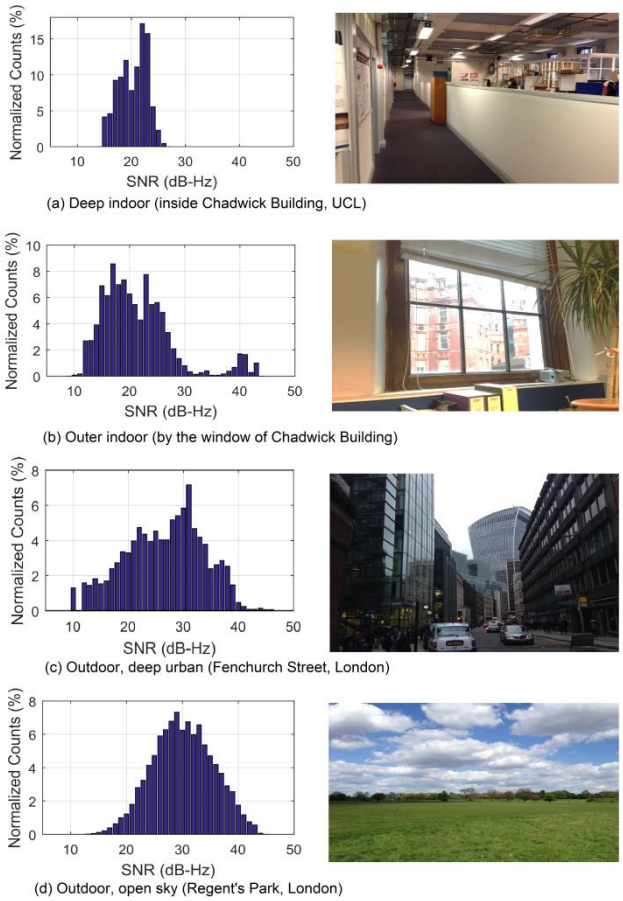

Figure 14. SNR measurement distributions under different environments

The number of satellites received and the total measured SNR, summed across all the satellites received at each epoch, were considered as features for the environmental classification algorithm. However, these were found to be poor at distinguishing the outer indoor and deep urban environments [2].

As a larger percentage of weak signals (less than 25 dB-Hz) are received indoors than outdoors, it was found that the differences in the classification features between environments are greater if these signals are deducted from the observations. Therefore context detection here is based on two features:

- The total number of GNSS signals received with an SNR of 25 dB-Hz or more, numSNR25;
- The sum of the SNRs of the GNSS signals received with an SNR of 25 dB-Hz or more, sumSNR25.

These features are plotted in Figure 15 for the test environments shown in Figure 14, demonstrating that all four environments can be distinguished using these features.

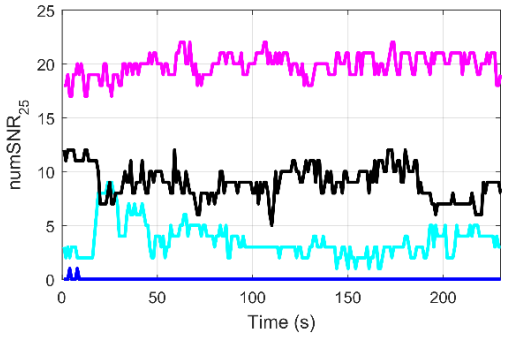

(a) Number of satellites with signals above 25 dB-Hz

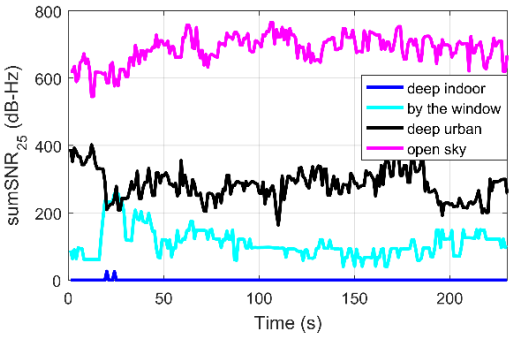

(b) Total SNR, summed across the signals above 25 dB-Hz

Figure 15. Features based on signals above 25 dB-Hz

In reality, the boundaries between indoor and outdoor environment can be ambiguous, rendering some scenarios hard to classify as either one. For a practical detection system, an uncertain decision is better than a wrong classification. Because an uncertain environment decision can be used in other ways (e.g. environment connectivity, environment and behaviour association) to improve the classification, but a wrong classification cannot. Similarly, it is better to inform a context-adaptive navigation system that the environment is uncertain than to provide it with an incorrect context. Therefore, to have a smooth transition between indoor and outdoor categories and reduce the likelihood of wrong classification, a new environment category of "intermediate" is introduced to serve as a bridge between the indoor and outdoor categories. The portico of UCL's Wilkins building, shown in Figure 16, is a typical example of an intermediate environment. This is covered by the roof of the building, but there is only one wall and the other three sides of this area are open.

Figure 16. The portico of UCL's Wilkins building, an example of the intermediate category

The features $numSNR_{25}$ and $sumSNR_{25}$ can be computed sequentially from the outputs of a GNSS receiver module. A hidden Markov model (HMM) is used in this study to determine the environmental context by integrating the observations over time.

The HMM assumes a Markov process with the states that cannot be visible directly [44] (indoor, intermediate or outdoor environment in this study), so that it is capable of modelling the inherent dynamic temporal relationships of environments. In general, a HMM comprises the following five elements [2]:

1) The state space **S** that consists of N hidden states $\mathbf{S}=\{S_1, S_2,\ldots, S_N\}$. In this research, there are only three hidden states: indoor, intermediate and outdoor, which are denoted as S_1, S_2 and S_3 respectively. At each epoch k, the probabilities that the system is in each state sum to unity.

2) The set of observations at each epoch k, $Z_k= \{z_{1,k}, z_{2,k},\ldots, z_{\ell,k},\ldots, z_{m,k}\}$, where $z_{\ell,k}$ is the ℓ-th observation at epoch k and m is the number of observations. In this study, $z_{1,k}$ refers to $numSNR_{25}$ while $z_{2,k}$ is $sumSNR_{25}$.

3) The matrix of state transition probabilities $\mathbf{A}=\{A_{ij}\}$. Each element of the state transition probabilities matrix, A_{ij}, defines the probability that the state transits from a value S_i at the immediately prior epoch to another value S_j at the current epoch. The following values are assumed:

k / k+1	Indoor	Intermediate	Outdoor
Indoor	2/3	1/3	0
Intermediate	1/3	1/3	1/3
Outdoor	0	1/3	2/3

4) The vector of emission probabilities $B=\{B_i(k)\}$ that defines the conditional distributions $P(Z_k|S_i)$ of the observations from a specific state. The following values are assumed where $N(\mu, \sigma^2)$ denotes a normal distribution with mean μ and variance σ^2.

$$P(z_{1,k} \mid X_k = S_1) \sim N(4,1.6)$$
$$P(z_{1,k} \mid X_k = S_2) \sim N(7.5,1.36)$$
$$P(z_{1,k} \mid X_k = S_3) \sim N(9,4)$$

$$P(z_{2,k} \mid X_k = S_1) \sim N(50, 2500)$$
$$P(z_{2,k} \mid X_k = S_2) \sim N(150, 625)$$
$$P(z_{2,k} \mid X_k = S_3) \sim N(350, 5000)$$

5) An initial state probability distribution $\Pi=\{\Pi_i\}$ that defines the probability of being state S_i at the first epoch. The following values are assumed:

$$P(X_1 = S_1) = P(X_1 = S_3) = 0.25$$
$$P(X_1 = S_2) = 0.5$$

In this paper, we use the first-order HMM, which assumes the current environmental context is only affected by the immediate previous context. This is illustrated by Figure 17. Given the sequence of the observations, the most likely sequence of hidden states can be inferred using the Viterbi algorithm [44][45]. The probabilities of the model are determined as follows.

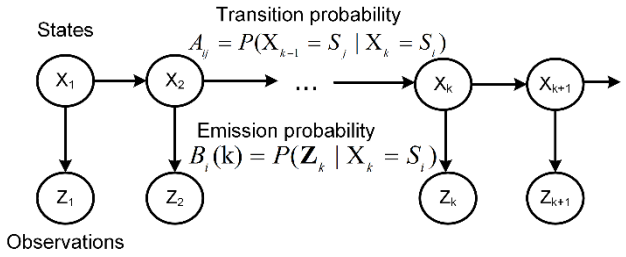

Figure 17. Structure of a first-order HMM

Four different kinds of environment types were chosen to test the detection ability of the proposed detection method under different GNSS reception conditions. The data for open sky (outdoor), deep urban (outdoor), outer indoor and deep indoor environments are as depicted in Figure 14. Figure 18 presents the detection results of the static experiments in different environments. In the case of open sky and deep indoor, the detection results are very accurate as all samples of these scenarios are successfully detected with almost 100% probability. Deep urban is a little challenging for the detector as more signals are blocked or reflected by the tall buildings around. It can be observed from the figure that most samples are classified to outdoor correctly but with some intermediate states occasionally appearing among them. A similar thing happens for the outer indoor environment by a window. As some direct signals can still be received by the window, the measurements between 20s and 30s are erroneously classified as an outdoor environment.

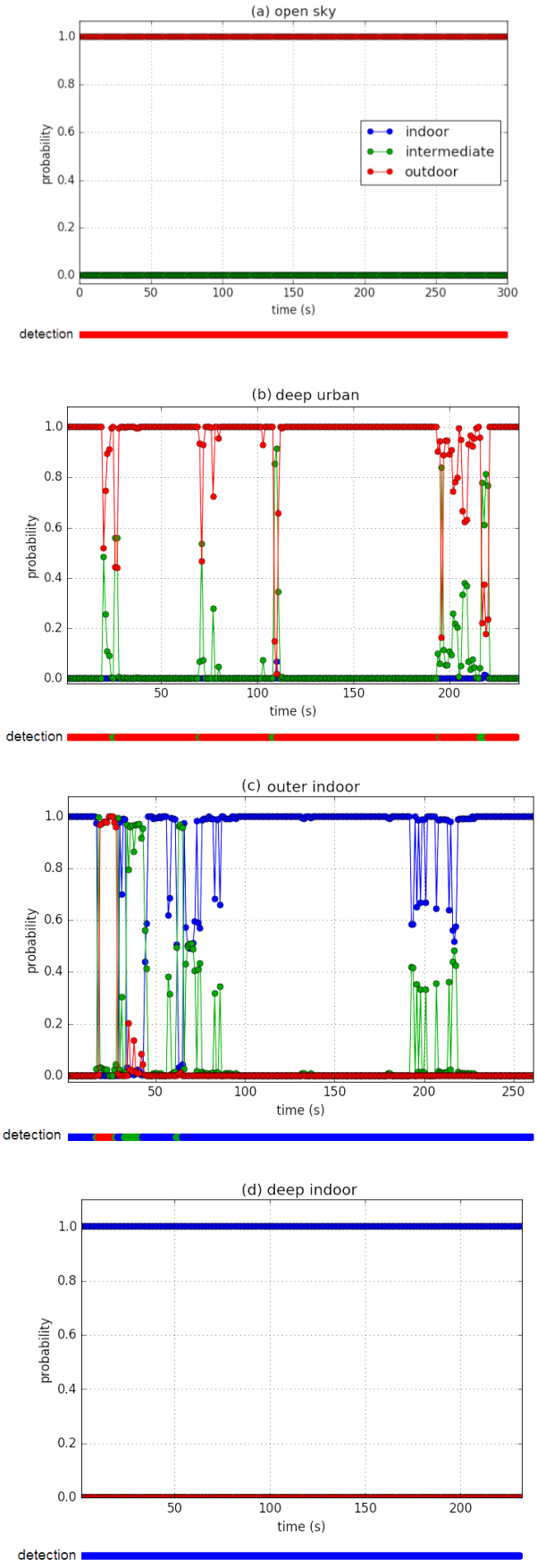

Figure 18. Static experiment results of the environment detection algorithm

6. CONCLUSIONS

A full implementation of the intelligent urban positioning 3D-mapping-aided GNSS concept has been presented, including a new likelihood-based 3DMA ranging algorithm and a hypothesis-based algorithm for integrating ranging with shadow matching. Both new algorithms have been shown to perform better than their predecessors.

The IUP algorithms were tested using data recorded using a u-blox EVK M8T consumer-grade GNSS receiver and a Nexus 9 tablet at 28 locations across two districts of London, representative of both traditional and modern dense urban environments. The Nexus 9 tablet used the Android Nougat GNSS receiver interface, so is representative of future smartphones. With the u-blox receiver, the single-epoch RMS horizontal (i.e., 2D) error across all sites was 4.0 m using the IUP algorithms, compared to 28.2 m for conventional positioning, a factor of 7.1 improvement. Using the Nexus tablet, the IUP RMS error was 7.0 m, compared to 32.7 m for conventional GNSS positioning, a factor of 4.7 improvement.

An analysis of processing and data requirements has shown that intelligent urban positioning is practical to implement in real-time on a mobile device or a server.

Finally, it has been shown that GNSS signals can be used to distinguish between indoor and outdoor environments.

6. FUTURE WORK

The following work is planned for the next year:

- Tests with a geodetic-grade GNSS receiver to determine the performance achievable with high-quality user equipment.
- Development of a real-time demonstration system using the Raspberry Pi and u-blox EVK 8MT platform.
- Extensive testing to quantify the effects of different error sources on both shadow matching and 3DMA GNSS ranging.
- Development of a multi-epoch version of the intelligent urban positioning algorithms presented here for both static and dynamic applications.
- Extend the GNSS-based environmental context determination algorithms to distinguish between different classes of outdoor environment in order to determine when the receiver is in an environment where it can benefit from intelligent urban positioning.

Longer term aspirations include:

- Implementation of outlier detection to compensate for out-of-date mapping and transient effects, such as passing buses.
- Computation of real-time performance metrics to provide rudimentary integrity.
- Integration of 3DMA GNSS with inertial sensors and other navigation technologies for added robustness.
- Further development of the shadow-matching algorithms as discussed in [22].
- Development of a full context-adaptive navigation system using both environmental and behavioural context.

ACKNOWLEDGEMENTS

The work on 3DMA GNSS is funded by the Engineering and Physical Sciences Research Council (EPSRC) project EP/L018446/1, *Intelligent Positioning in Cities using GNSS and Enhanced 3D Mapping*. The project is also supported by Ordnance Survey, u-blox and the Royal National Institute for Blind People.

The work on context determination is funded by the UCL Engineering Faculty Scholarship Scheme and the Chinese Scholarship Council. The authors would like to thank Dr. Mark Herbster and Dr. Simon Julier of UCL's Department of Computer Science for their useful comments and suggestions.

REFERENCES

[1] Adjrad, M. and Groves, P. D., "Intelligent Urban Positioning using Shadow Matching and GNSS Ranging," Portland, Oregon. Also available from http://discovery.ucl.ac.uk/.

[2] Gao, H. and Groves, P. D., "Context Determination for Adaptive Navigation using Multiple Sensors on a Smartphone," Portland, Oregon. Also available from http://discovery.ucl.ac.uk/.

[3] Groves, P. D., "GNSS Solutions: Multipath vs. NLOS signals. How Does Non-Line-of-Sight Reception Differ From Multipath Interference," *Inside GNSS Magazine*, Nov/Dec 2013, pp. 40-42, 63.

[4] Groves, P. D., *Principles of GNSS, inertial, and multi-sensor integrated navigation systems*, Second Edition, Artech House, 2013.

[5] Bhuiyan M. Z. H. and Lohan, E. S., "Multipath Mitigation Techniques for Satellite-Based Positioning Applications," in Jin, S. (Ed.) *Global Navigation Satellite Systems: Signal, Theory and Applications*, InTech, 2012, pp. 405-426

[6] Groves, P. D. and Jiang, Z., "Height Aiding, C/N0 Weighting and Consistency Checking for GNSS NLOS and Multipath Mitigation in Urban Areas". *Journal of Navigation*, 66, 2013, 653–669. Also available from http://discovery.ucl.ac.uk/.

[7] Amt, J. R. and Raquet, J. F., "Positioning for Range-Based Land Navigation Systems Using Surface Topography," *Proc. ION GNSS* 2006, Fort Worth, TX, 1494–1505.

[8] Adjrad, M., and Groves, P. D., "Enhancing Least Squares GNSS Positioning with 3D Mapping without

Accurate Prior Knowledge," Accepted for publication in *NAVIGATION*, 2016.

[9] Bradbury, J., Ziebart, M., Cross, P. A., Boulton, P. & Read, A., "Code Multipath Modelling in the Urban Environment Using Large Virtual Reality City Models: Determining the Local Environment". *Journal of Navigation*, 60(1), 2007, 95-105.

[10] Suh, Y. and Shibasaki, R.., "Evaluation of satellite-based navigation services in complex urban environments using a three-dimensional GIS". *IEICE Transactions on Communications*, E90-B**,** 2007, 1816-1825.

[11] Wang, L., Groves, P. D. and Ziebart, M. K., "Multi-Constellation GNSS Performance Evaluation for Urban Canyons Using Large Virtual Reality City Models," *Journal of Navigation*, 65(3), 2012, 459–476. Also available from http://discovery.ucl.ac.uk/.

[12] Groves, P. D., "Shadow Matching: A New GNSS Positioning Technique for Urban Canyons". *Journal of Navigation*, 64(3), 2011, 417-430. Also available from http://discovery.ucl.ac.uk/.

[13] Ben-Moshe, B., et al., "Improving Accuracy of GNSS Devices in Urban Canyons". *23rd Canadian Conference on Computational Geometry*, 2011.

[14] Wang, L., Groves, P. D. and Ziebart, M. K., "GNSS Shadow Matching Using A 3D Model of London". *European Navigation Conference*, London, 2011. Also available from http://discovery.ucl.ac.uk/.

[15] Suzuki, T., and Kubo, N., "GNSS Positioning with Multipath Simulation using 3D Surface Model in Urban Canyon". *ION GNSS* 2012, Nashville, TN.

[16] Wang, L., Groves, P. D. and Ziebart, M. K., "GNSS Shadow Matching: Improving Urban Positioning Accuracy Using a 3D City Model with Optimized Visibility Prediction Scoring". *NAVIGATION*, 60(3), 2013, 195–207. (First published at *ION GNSS*, 2012, Nashville, TN). Also available from http://discovery.ucl.ac.uk/.

[17] Isaacs, J. T., Irish, A. T., et al., "Bayesian localization and mapping using GNSS SNR measurements". *IEEE/ION PLANS* 2014. Monterey, California.

[18] Wang, L., Groves, P. D. and Ziebart, M. K., "Smartphone Shadow Matching for Better Cross-street GNSS Positioning in Urban Environments". *Journal of Navigation*, 68(3), 2015, 411–433. Also available from http://discovery.ucl.ac.uk/.

[19] Wang, L., *Investigation of Shadow Matching for GNSS Positioning in Urban Canyons*, PhD Thesis, University College London, 2015. Available from http://discovery.ucl.ac.uk/.

[20] Yozevitch, R. and Ben-Moshe, B., "A Robust Shadow Matching Algorithm for GNSS Positioning," *NAVIGATION*, 62(2), 2015, 95–109.

[21] Wang, L., Groves, P. D. and Ziebart, M. K., "Urban Positioning on a Smartphone: Real-time Shadow Matching Using GNSS and 3D City Models". *ION GNSS+* 2013, Nashville, Tennessee. AND *Inside GNSS*, Nov/Dec 2013, 44–56. Also available from http://discovery.ucl.ac.uk/.

[22] Groves, P. D., Wang, L., Adjrad, M., and Ellul, C., "GNSS Shadow Matching: The Challenges Ahead". *ION GNSS+* 2015, Tampa, Florida. Also available from http://discovery.ucl.ac.uk/.

[23] Obst, M., S. Bauer, and G. Wanielik, "Urban Multipath Detection and mitigation with Dynamic 3D Maps for Reliable Land Vehicle Localization," *IEEE/ION PLANS* 2012.

[24] Bourdeau, A. and Sahmoudi, M., "Tight Integration of GNSS and a 3D City Model for Robust Positioning in Urban Canyons". *ION GNSS* 2012, Nashville, Tennessee.

[25] Peyraud, S., et al., "About Non-Line-Of-Sight Satellite Detection and Exclusion in a 3D Map-Aided Localization Algorithm," *Sensors*, Vol. 13, 2013, pp. 829-847.

[26] Suzuki, T., "Integration of GNSS Positioning and 3D Map using Particle Filter" *ION GNSS+* 2016, Portland, Oregon.

[27] Suzuki, T., and Kubo N., "Correcting GNSS Multipath Errors Using a 3D Surface Model and Particle Filter," *ION GNSS+* 2013, Nashville, TN.

[28] Kumar, R. and Petovello, M, G., "A Novel GNSS Positioning Technique for Improved Accuracy in Urban Canyon Scenarios using 3D City Model", *ION GNSS+* 2014, Tampa, FL.

[29] Hsu, L.-T., Gu, Y., and Kamijo, S., "3D building model-based pedestrian positioning method using GPS/GLOANSS/QZSS and its reliability calculation", *GPS Solutions*, 2015, doi 10.1007/s10291-015-0451-7.

[30] Kumar, R. and Petovello, M, G., "Sensitivity Analysis of 3D Building Model-assisted Snapshot Positioning", *ION GNSS+* 2016, Portland, Oregon.

[31] Betaille, D., et al., "A New Modeling Based on Urban Trenches to Improve GNSS Positioning Quality of Service in Cities". *IEEE Intelligent Transportation Systems Magazine*, 5(3), 2013, 59–70.

[32] Ng, Y. and Gao, G. X., "Direct Positioning Utilizing Non Line of Sight (NLOS) GPS Signals", *ION GNSS+* 2016, Portland, Oregon.

[33] Groves, P. D., Jiang, Z., Wang, L. and Ziebart, M., "Intelligent Urban Positioning using Multi-Constellation GNSS with 3D Mapping and NLOS Signal Detection". *ION GNSS* 2012. Nashville, Tennessee. Also available from http://discovery.ucl.ac.uk/.

[34] Adjrad, M., and Groves, P. D., "Intelligent Urban Positioning: Integration of Shadow Matching with

3D-Model-Aided GNSS Ranging," *Submitted for journal publication*, 2016. Please email the authors to obtain a copy before publication.

[35] Lin, T., C. O'Driscoll, and G. Lachapelle, "Channel Context Detection and Signal Quality Monitoring for Vector-based Tracking Loops," *Proc. ION GNSS 2010*.

[36] Lin, T., C. O'Driscoll, and G. Lachapelle, "Development of a Context-Aware Vector-Based High-Sensitivity GNSS Software Receiver," *Proc. ION ITM*, Jan. 2011.

[37] Groves, Paul D., et al. "Context detection, categorization and connectivity for advanced adaptive integrated navigation." *ION GNSS+ 2013*.

[38] Groves, Paul D., et al. "The four key challenges of advanced multisensor navigation and positioning." *IEEE/ION PLANS 2014*.

[39] Shafiee, M., K., O'Keefe, and G. Lachapelle, "Context-aware Adaptive Extended Kalman Filtering Using Wi-Fi Signals for GPS Navigation," *Proc. ION GNSS 2011*.

[40] Adjrad, M., and Groves, P. D., "Enhancing Conventional GNSS Positioning with 3D Mapping without Accurate Prior Knowledge". *ION GNSS+* 2015, Tampa, Florida. Also available from http://discovery.ucl.ac.uk/.

[41] Groves, P. D., "It's Time for 3D-Mapping-Aided GNSS". *Inside GNSS*, Sep/Oct 2016.

[42] OGC 2015, *CityGML Standard, Open Geospatial Consortium*, http://www.opengeospatial.org/ standards/citygml [Accessed 3rd February 2015]

[43] Kolbe, T. H., Groger, G. and Plumer, L., "CityGML: Interoperable access to 3D city models." In: *Geo-information for disaster management*, Springer, 2005, 883–899.

[44] Bishop, Christopher M., *Pattern recognition and machine learning*. Company New York, 2006.

[45] Viterbi, Andrew J. "Error bounds for convolutional codes and an asymptotically optimum decoding algorithm." *Information Theory, IEEE Transactions on* 13.2 (1967): 260-269.